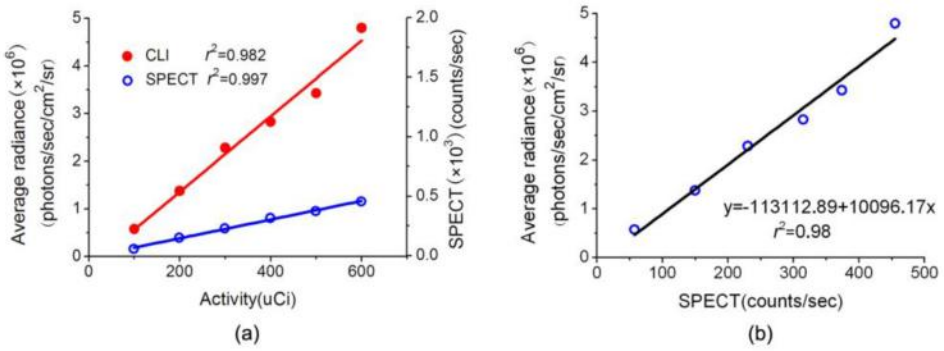

Fig. 2. Correlation analysis between Cerenkov luminescence imaging (CLI) and SPECT imaging. (a) Quantification of imaging signals showed a drastic increase from 100 μCi to 600 μCi. (b) Quantification of signals showed a robust *in vitro* correlation between CLI and SPECT imaging (r^2 = 0.98).

3.2 In vivo 3D CLT based on a heterogeneous mouse model

To perform *in vivo* 3D CLT of an electron-emitting radiotracer based on a heterogeneous animal model, an adult athymic nude mouse with an implanted $Na^{131}I$ radioactive source was imaged with a dual-modality ZKKS-Direct3D molecular imaging system (jointly developed by Guangzhou Zhongke Kaisheng Medical Technology CO., Ltd, Xidian University and Institute of Automation, CAS). This system is comprised of an optical imaging system and a micro-CT system. The central piece of the system is an animal-imaging holder which is used to affix the anesthetized mouse. The optical imaging system employs a scientific liquid–cooled back illuminated CCD camera (Princeton Instruments PIXIS 2048B, Roper Scientific, Trenton, NJ) coupled with an imaging lens (Nikon Normal Macro 55 mm *f*/2.8). The CCD camera generates 2048 × 2048 16-bit images with a 13.5 μm × 13.5 μm pixel size. The micro-CT system consists of a micro-focus X-ray source (Oxford Instruments Series5000 Apogee, CA) with a 35 μm focal spot size, a tuning range of 4 to 50 kVp voltage, and 0 to 1.0 mA current; along with an X-ray detector (HAMAMATSU C7921CA-02, Hamamatsu, Japan) with a voltage detection range from 20 to 100 kVp with a 50 μm × 50 μm pixel size.

In the experiment, an adult male athymic nude mouse underwent aseptic celiotomy. The animal received isoflurane (2%) for general anesthesia. A radioactive source made of a glass vessel that was filled with approximately 600 μCi $Na^{131}I$ was implanted in the abdomen. The radioactive source was dipped in alcohol for <20 min for antisepsis before implantation. All animal procedures were in accordance with the Fourth Military Medical University (FMMU) approved animal protocol. After implantation, the mouse was affixed to the animal-imaging holder and placed on the rotation stage. The rotation stage was vertically rotated under computer control for acquisition of multi-view luminescent images and micro-CT projection data. Luminescent images were acquired using a 675-775 nm filter with a binning value of 4, integration time of 5 min and aperture number f_{num} = 8. Figure 3(a)-(d) shows the four luminescent images superimposed on the corresponding photographs in the anterior-posterior, left lateral, right lateral, and posterior-anterior views respectively. For acquiring structural information from biological tissues, the mouse was scanned by the micro-CT system in the vertical position immediately after celiac administration of the contrast material iohexol using the following imaging parameters: 40 kVp, 700 μA, and a 5 min scan.

#131117 - $15.00 USD Received 6 Jul 2010; revised 8 Sep 2010; accepted 2 Nov 2010; published 9 Nov 2010

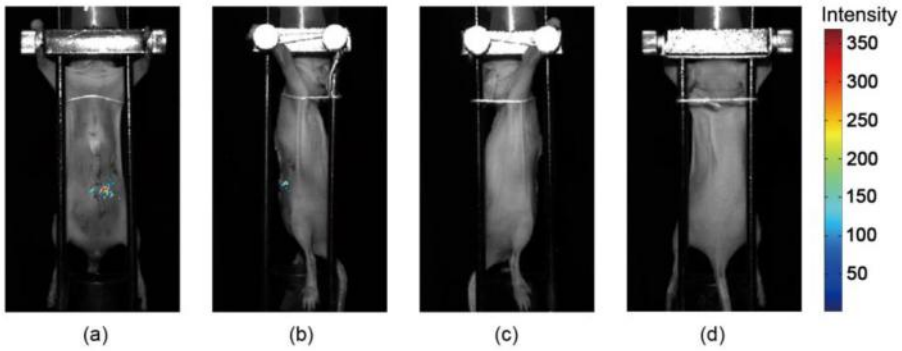

Fig. 3. Luminescent views in pseudo-color superimposed on the corresponding photographs of the mouse with an implanted 600 μCi $Na^{131}I$ radioactive source. (a)-(d) Anterior-posterior, left lateral, right lateral, and posterior-anterior views respectively.

Reconstructed CT images were segmented into several major anatomical components including adipose, heart, lungs, liver, stomach, and kidneys. A geometrical model of the mouse was generated consisting of 26640 tetrahedral elements and 4980 nodes as shown in Fig. 4(a). The acquired 2D luminescence images on the CCD camera were mapped onto the 3D mesh surface of the geometrical model using the method proposed in [25] as shown in Fig. 4(b). Based on the light flux distribution on the surface, an initial permissible source region was selected as $\Omega = \{(x, y, z) | 17 < x < 27, 20 < y < 29, 4 < z < 16\}$. Optical parameters of biological tissues at wavelengths of 675-775 nm were calculated based on literature [26].

Using the adaptive *hp*-FEM algorithm [11], the 3D distribution information of an internal $Na^{131}I$ radioactive source was reconstructed as shown in Fig. 5(a). In order to analyze the results quantitatively, we defined the distance error $d = \sqrt{(x-x_0)^2 + (y-y_0)^2 + (z-z_0)^2}$, where (x, y, z) was the coordinate of the reconstructed source with maximum density, and (x_0, y_0, z_0) was that of the actual source. The position of the actual source could be obtained by the micro-CT images as (24.80, 21.90, 9.30) mm, and the location of the reconstructed source was (23.17, 20.50, 9.23) mm. The distance error was 2.15 mm. In addition, we performed CLT based on a homogeneous mouse model. A 3D rendering of the reconstructed source distribution in the homogeneous mouse model is shown in Fig. 5(b). The distance error between the actual source and the reconstructed one was 4.41 mm. Comparison of the reconstruction results based on the heterogeneous and homogeneous mouse models are listed in Table 1, which demonstrates that the reconstruction results based on the heterogeneous mouse model are more accurate in localization than the homogeneous one. Figure 5(c) shows the micro-CT slice fused with the reconstructed source (red triangle) based on the heterogeneous mouse model from a sagittal view. We also found that the reconstructed source based on the heterogeneous mouse model was very close to the location of the implanted source (inside the black circle). Our data showed the ability of *in vivo* CLT to recover the radioactive probe distribution in a heterogeneous mouse model.

#131117 - $15.00 USD Received 6 Jul 2010; revised 8 Sep 2010; accepted 2 Nov 2010; published 9 Nov 2010

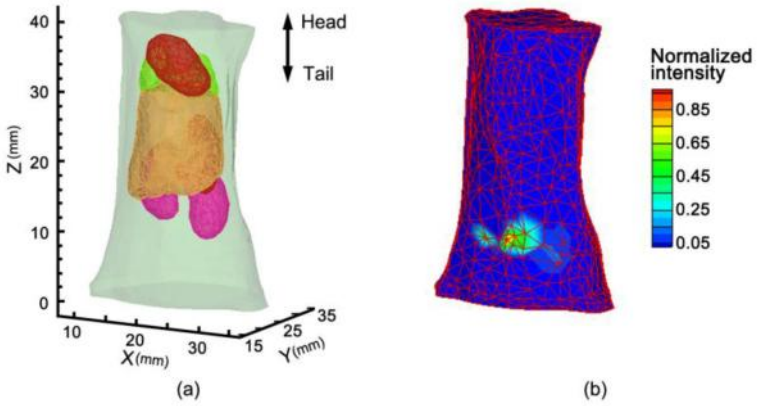

Fig. 4. Mouse model with an implanted 600 μCi $Na^{131}I$ radioactive source and its associated luminescent measurement. (a) A geometrical model of the mouse chest consisting of adipose, heart, lungs, liver, stomach, and kidneys. (b) The measured luminescent data mapped onto the 3D mesh surface of the mouse chest.

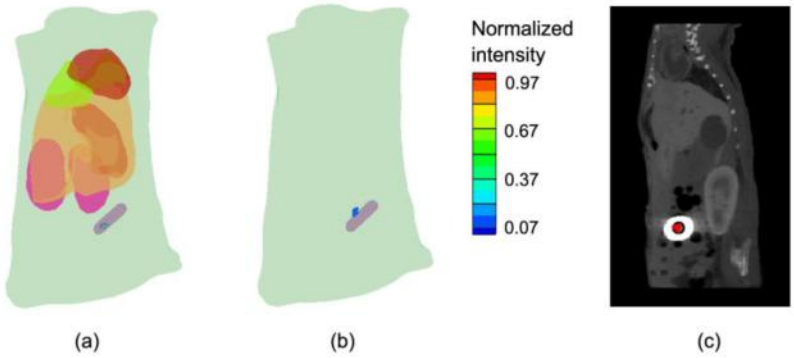

Fig. 5. CLT reconstruction of the radioactive source distribution in the mouse with an implanted 600 μCi $Na^{131}I$ radioactive source. (a) and (b) are the 3D renderings of the reconstructed source distribution in heterogeneous and homogeneous mouse models respectively. (c) The true source (inside the black circle) in a micro-CT slice superimposed with the reconstructed source (red triangle) from a sagittal view.

Table 1. Comparison of reconstruction results based on heterogeneous and homogeneous mouse models

Mouse model	Actual source center (mm)	CLT reconstructed location (mm)	*d* (mm)
Homogeneous	(24.80, 21.90, 9.30)	(20.83, 20.46, 10.58)	4.41
Heterogeneous	(24.80, 21.90, 9.30)	(23.17, 20.50, 9.23)	2.15

3.3 SPECT imaging validation experiment

In the previous section, we recovered the 3D distribution of an internal radioactive source, and the accuracy of the reconstructed result was confirmed by the micro-CT images. The *in vivo* CT imaging strategy is commonly used to validate artificial source-based optical experiments [13,14]. However, due to poor soft tissue contrast, it is difficult to determine the position of the tumor [14]. Cerenkov radiation based on radioactive molecular probes may help us solve this problem. The images of the subject labeled with a radioactive probe can be obtained both by nuclear imaging and optical imaging, which makes the nuclear imaging modality a useful validation tool. *In vivo* nuclear imaging modalities, including PET and SPECT, can obtain accurate functional information; if they are combined with the CT

#131117 - $15.00 USD Received 6 Jul 2010; revised 8 Sep 2010; accepted 2 Nov 2010; published 9 Nov 2010

modality, they can achieve 3D distribution of the molecular probes [27]. Therefore, they serve as an effective reference for optical imaging, especially for optical tomography.

In this study, we proposed a SPECT imaging validation strategy to verify the results of CLT. First, the same radioactive sources $Na^{131}I$ utilized in the *in vitro* imaging experiment were implanted into adult athymic nude mice abdomens (n = 6). The activities of the sources were 100 μCi, 200 μCi, 300 μCi, 400 μCi, 500 μCi and 600 μCi respectively. The mice were then imaged by the aforementioned IVIS system with a 695-770 nm filter (Cy5.5). The luminescent images were acquired with a binning value of 4, integration time of 5 min and an aperture number f_{num} = 1. Next, the mice underwent SPECT imaging with the aforementioned SPECT-CT system for 20 min in the same supine position as for the optical acquisition, and images were reconstructed using a filtered back-projection algorithm. Using the previously described method, 3D distribution of an internal $Na^{131}I$ radioactive source was reconstructed.

The reconstruction results both in localization and intensity of the 300 μCi radioactive source are shown in Fig. 6. Figure 6(a) and Fig. 6(b) present the reconstruction results in horizontal, coronal, and sagittal views of CLT and SPECT imaging respectively. Comparison of the reconstruction results for all of the radioactive sources using CLT and SPECT imaging are listed in Table 2. The distance errors between the actual source, obtained from SPECT imaging, and the reconstructed one were acceptable. These data clearly showed the advantages of SPECT imaging validation for CLT and the potential to verify the results of optical molecular tomography. In addition, we further discussed the relationship between the radiotracer activity and the reconstructed maximum intensity. The maximum intensities of the reconstructed sources as a function of activity are depicted in Fig. 7. We found that the maximum intensity of the reconstructed source linearly increased with increasing activity. Moreover, there was a robust correlation between activity versus the maximum intensity (r^2 = 0.966). Our results suggested that localization and intensity of an embedded radioactive source with various concentrations could be recovered with certain accuracy.

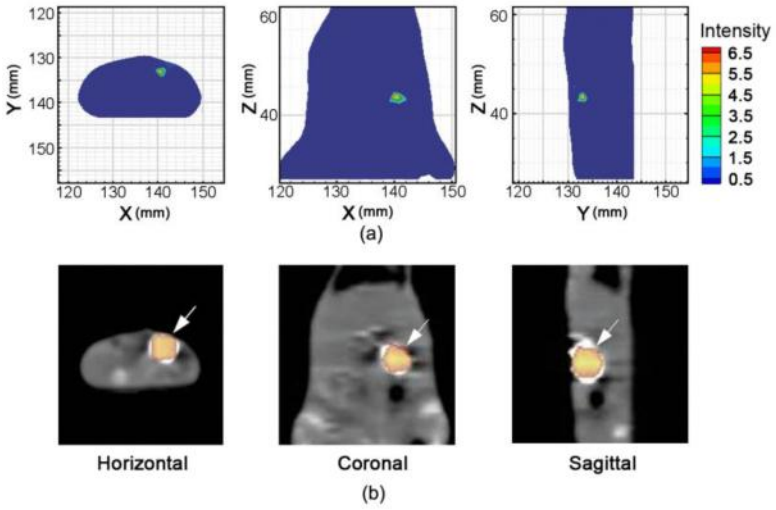

Fig. 6. The reconstruction results of the 300 μCi $Na^{131}I$ radioactive source. (a) and (b) are the reconstruction results in horizontal, coronal, and sagittal views of CLT and SPECT imaging respectively. Fusion of the reconstruction source with SPECT and CT images shows the exact SPECT reconstruction location of the implanted radioactive source (arrow). The images are shown in horizontal, coronal, and sagittal views.

#131117 - $15.00 USD Received 6 Jul 2010; revised 8 Sep 2010; accepted 2 Nov 2010; published 9 Nov 2010

Table 2. Comparison of reconstruction results obtained using CLT and SPECT

Radioactivity of source (μCi)	SPECT reconstructed location (mm)	CLT reconstructed location (mm)	*d* (mm)	CLT reconstructed maximum intensity
100	(76.82, 69.80, 31.50)	(76.43, 68.63, 32.17)	1.40	0.16
200	(100.90, 90.30, 28.00)	(102.32, 88.78, 27.94)	2.08	2.36
300	(140.00, 133.00, 43.00)	(140.10, 132.87, 43.42)	0.45	6.69
400	(102.87, 95.10, 32.00)	(101.80, 93.90, 33.50)	2.20	14.23
500	(96.11, 73.25, 29.00)	(96.49, 75.09, 30.46)	2.38	28.73
600	(87.44, 91.42, 26.00)	(88.11, 91.41, 26.46)	0.81	37.57

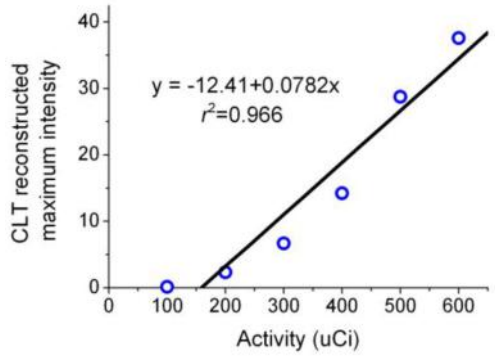

Fig. 7. Correlation analysis between CLT reconstructed maximum intensity and the radiotracer activity. There was a robust correlation between activity versus the maximum intensity (r^2 = 0.966).

4. Discussion and conclusions

Among the imaging modalities that can be used for noninvasive molecular imaging, optical imaging holds an important role in animal research because of its low cost, high sensitivity and molecular specificity [2,3]. We believe that research in optical imaging based on Cerenkov radiation will open new avenues for *in vivo* molecular imaging in small animals.

In vitro experiments showed that the radioactive sources emitted a mass of light and the measured spectrum presented a broad and continuous distribution from 500 nm to 900 nm, similar to previous studies [15,17,18]. Both of the results showed that the emitted light from $Na^{131}I$ was correlated with Cerenkov radiation, and Cerenkov photon migration in tissues can be described by DE with acceptable accuracy. Moreover, *in vitro* experiments showed that there was a robust correlation between the optical signal versus the nuclear signal (r^2 = 0.98), thus Cerenkov luminescence imaging could reflect similar information as SPECT imaging.

In this study, we performed *in vivo* CLT based on a heterogeneous mouse model with an implanted $Na^{131}I$ radioactive source. Li *et al*. presented CLT based on a homogeneous mouse model [19]. However, the assumption of a homogeneous optical property background will lead to inaccurate source reconstruction [22,26]. Our results showed that the reconstruction based on a heterogeneous mouse model was more accurate in localization than using the homogeneous one.

Moreover, a SPECT imaging validation strategy was also presented, in which SPECT imaging was regarded as a criterion. The distance errors between the actual source from SPECT imaging and the reconstructed one of CLT were acceptable. These data showed the strength of the SPECT imaging validation strategy for CLT, and its potential for verifying the results of optical tomography. In addition, localization and intensity of an embedded radioactive source with variable concentrations were recovered with certain accuracy, and a robust correlation between activity versus the reconstructed maximum intensity (r^2 = 0.966) was obtained.

#131117 - $15.00 USD Received 6 Jul 2010; revised 8 Sep 2010; accepted 2 Nov 2010; published 9 Nov 2010

Normally, optical imaging is used to detect visible or near-infrared light produced by fluorescent or bioluminescent probes. These imaging probes might hinder optical imaging application in clinics due to their potential toxicities. Radiotracers, such as [^{18}F]-FDG, Na^{18}F, and Na^{131}I, have been developed for PET or SPECT imaging, which have been widely used in clinics for the past several years. Cerenkov radiation based on radioactive probes relieves optical imaging from potential toxicities in traditional optical probes, opening new venues for preclinical research.

In conclusion, *in vivo* 3D CLT of small living animals demonstrated the ability of *in vivo* CLT to recover radioactive probe distribution in a heterogeneous mouse model. Moreover, this study showed the strength and benefit of the SPECT imaging validation strategy for CLT. Our future work will focus on the applications of this new imaging modality on tumor-bearing mice using radioactive probes.

Acknowledgements

We acknowledge Rongqing Zhang (Department of Cardiology, Xijing Hospital, Fourth Military Medical University), Runqiang Han, Kuan Peng, Nunu Ren, and Wei Li (Life Sciences Research Center, School of Life Sciences and Technology, Xidian University) during these experiments. This work is supported by the Program of the National Basic Research and Development Program of China (973) under Grant Nos. 2006CB705700, 2011CB707702, CAS Hundred Talents Program, the National Natural Science Foundation of China under Grant Nos. 81090272, 81000632, 30900334, the Shaanxi Provincial Natural Science Foundation Research Project under Grant No. 2009JQ8018, and the Fundamental Research Funds for the Central Universities.

#131117 - $15.00 USD Received 6 Jul 2010; revised 8 Sep 2010; accepted 2 Nov 2010; published 9 Nov 2010